Physics and Chemistry of the Earth 53–54 (2012) 19–29

Contents lists available at SciVerse ScienceDirect

Physics and Chemistry of the Earth

journal homepage: www.elsevier.com/locate/pce

Modeling and assessing hydrologic processes for historical and potential land-cover change in the Duoyingping watershed, southwest China

Xingnan Zhang [a,b], Yangyang Liu [a,*], Yuanhao Fang [a], Bojuan Liu [a], Dazhong Xia [a]

[a] College of Hydrology and Water Resources in Hohai University, No. 1, Xikang Road, Nanjing 210098, China
[b] National Engineering Research Center of Water Resources Efficient Utilization and Engineering Safety, Hohai University, No. 1, Xikang Road, Nanjing 210098, China

ARTICLE INFO

Article history:
Available online 7 September 2011

Keywords:
Land-cover change
Scenario
Variable Infiltration Capacity
Hydrologic processes

ABSTRACT

Land-cover change significantly influences hydrologic processes at the watershed level. The mountainous Duoyingping watershed in upstream Yangtze River, China, has undergone dramatic land-cover change in the past three decades. It is likely to maintain this trend in the future, inevitably altering hydrologic processes in the region to a certain degree. Therefore, the effects of land-cover change on runoff, evapotranspiration (ET), and soil moisture in the watershed were assessed using a large-scale Variable Infiltration Capacity (VIC) hydrologic model.

To minimize the effect of climate change on simulation results, we used detrended climate data over the period 1980–2005 in forcing the VIC model. The dynamics in the spatial distribution of land-cover types in the Duoyingping watershed from 1980 to 2000 were first examined, revealing that reforestation and deforestation were the major change patterns. On the basis of various land-use policies, potential land-cover scenarios for 2030 were established using an integrated land-use change model (CLUE-S). The scenarios were developed using 2000 land-use data as bases. Finally, the calibrated VIC model was applied in the scenarios to assess land-cover effects on hydrology. Hydrologic simulations showed that the effects of historical land-cover change on hydrology were discernible in the sub-watersheds of Nanba, Yingjing, and Yuxi. The annual ET was projected to decrease by 0.8–22.3% because of deforestation, and increase by 2.3–27.4% because of shrubland–forest conversion. Different potential land-cover scenarios play various roles in the effect on hydrology because of various land-use policies. In the scenario concerning forest protection policy, annual ET increased by more than 15%, while annual runoff decreased by 6%. However, a negligible effect on hydrology was found under the scenario involving cropland expansion. On the basis of the results, it is concluded that ET is more sensitive to land-cover change than are other hydrologic components. Hydrologic alteration caused by reforestation and deforestation during the dry season was more significant than that during wet season. Generally, the proposed approach in the study can be a useful means of assessing hydrologic responses to land-cover change.

1. Introduction

Land-cover plays a significant role in water resource conservation and ecological protection in a mountainous watershed because of the vulnerability of mountain ecosystems. Changes in vegetation cover can affect runoff generation and concentration by altering hydrologic processes such as evapotranspiration (ET), infiltration, soil moisture content, and canopy interception, thereby influencing the magnitude of deterioration in water quality and spatial distribution of water resources in a watershed. Many previous studies found that land-cover change has become a dominant factor that shapes landscape characteristics, such as surface roughness, Leaf Area Index (LAI), and surface albedo (ALB), which can be critical to hydrologic processes (Mao and Cherkauer, 2009; Matheussen et al., 2000; VanShaar et al., 2002). Therefore, a thorough understanding of land-cover dynamics is necessary for reconstructing past land-cover scenarios and predicting potential scenarios. Scenario development may facilitate the quantitative assessment of hydrologic responses to changes in vegetation cover.

At different watershed scales, numerous researchers have developed various methods with the aim of quantifying the hydrologic alterations that were believed to be suitable for study in relation to land-cover change. Generally, the methods for detecting hydrologic responses to land-use/cover focus mainly on three aspects, namely, (a) field-based experimentation for comparison, (b) statistical analysis based on observations, and (c) hydrologic modeling under different scenarios.

For field-based experimentation, Germer et al. (2010) investigated hydrologic alterations caused by deforestation in pastures

* Corresponding author. Tel.: +86 15850589570; fax: +86 (0)25 83786609.
E-mail address: lyyang@foxmail.com (Y. Liu).

1474-7065/$ - see front matter © 2011 Elsevier Ltd. All rights reserved.
doi:10.1016/j.pce.2011.08.021

by comparing the results in an Amazon forest with those in an adjacent pasture shifted from the same forest 25 years ago on the basis of field measurements. Moreover, plot-based experiments at four sites that transitioned from grassland to shrubland in New Mexico were designed to examine spatio-temporal changes in soil moisture, runoff, and erosion (Turnbull et al., 2010).

For statistical analysis, using the observations from the US Geological Survey (USGS) gauging stations and historical land-use change records in the Mississippi River (MR) Basin as bases, Zhang and Schilling (2006) attempted to determine the relationship between increasing river flow (especially baseflow) and land-use change that occurred in the MR Basin over the last 60 years. They specifically studied the changes in ET, groundwater recharge, baseflow, and streamflow induced by the conversion of perennial vegetation to seasonal row crops (especially soybeans) in the basin since the 1940s. Schilling et al. (2010) extended the previous work by quantifying the actual effects of increased soybean cultivation on changes in the relationship between discharge and precipitation, while other researchers looked into how watershed degradation influenced water resources (Bewket and Sterk, 2005).

Scenario-based hydrologic modeling has been widely applied in investigating hydrologic responses to land-use/cover change. In most studies, historical and present land-use/cover patterns or extreme scenarios are always used as input in hydrologic models to determine hydrologic responses to different scenarios (Bowling et al., 2000; Fohrer et al., 2001; Ghaffair et al., 2010; Hong et al., 2010; Lørup et al., 1998; Legesse et al., 2003; Moiwo et al., 2010; Pfister et al., 2004; Savary et al., 2009). For instance, Storck et al. (1998) used the distributed hydrology soil vegetation model to assess the hydrologic effects of logging in the Pacific Northwest. Hundecha and Brdossy (2004) attempted to regionalize the parameters of a conceptual rainfall–runoff model with the aim of assessing the effects of different land-use scenarios generated in the model area on runoff generation in selected catchments of the Rhine Basin. These studies provided feasible ways to address hydrologic and water resources problems caused by changing environments; many useful conclusions have been drawn.

Nevertheless, the manner by which effective methodologies are adopted in assessing the effects of potential land-use/cover change on hydrology remains a problem that urgently requires resolution. To address this issue, combining a land-use change model and a hydrologic model appears to be a novel approach, yet only a few researchers have employed this technique, which is based on various land-use change models (Chen et al., 2009; Chu et al., 2010; Lin et al., 2007, 2008; Niehoff et al., 2002). A wide range of land-use/cover change models, including stochastic, empirical, dynamic, and integrated models, have been developed; however, simulations in which an integrated model is used to examine the dynamics of land-use/cover constantly prove superior because input data are readily available and the model features simple operation.

The Duoyingping (DYP) watershed is one of the most important forest regions in China. This region has undergone complex land-cover change over the last several decades, and the policies on *Grain-for-Green and Soil Erosion Control* are thought to further exacerbate these changes. These historical and potential changes in vegetation cover and their possible effects on hydrology necessitate thorough investigation.

In this paper, a macro-scale Variable Infiltration Capacity (VIC) hydrologic model was first applied to the DYP watershed under historical land-cover scenarios to analyze how and to what degree the changes in land-cover have affected regional hydrology. Detrended climate data were used as bases for the analysis. Then, we simulated future land-cover scenarios using the integrated CLUE-S model based on a logistic regression analysis under different land-use demand policies. Land-cover scenarios obtained using the CLUE-S were coupled with those derived from the VIC model to simulate runoff (surface runoff and baseflow), ET, and soil moisture. We also investigated the actual effects of potential land-cover changes on hydrologic processes in the studied watershed.

2. Methodology

2.1. Hydrologic model

The VIC model (Liang et al., 1994) is based on a soil–vegetation–atmosphere transfer scheme, which takes both water and energy balances into account. This model adopts a spatially varying infiltration curve to represent subgrid infiltration variability, and the baseflow is represented as a nonlinear recession following the Arno model (Franchini and Pacciani, 1991). Latent and sensible heat are calculated using the aerodynamics model.

Each grid cell's land cover can be horizontally subdivided into $N+1$ "tiles," where $n = 1, 2 \ldots, N$ represents N different types of vegetation, and $n = N+1$ represents bare soil. In the vertical direction, each grid is subdivided into canopy and three-layer soil in the new version of the VIC-3L model (Liang et al., 1996a,b). The top two soil layers (upper soil layer) are used to depict the dynamic response of soil to precipitation, while the third soil layer (lower soil layer) can reflect the gradual variations between storm and soil moisture. Depending on different vegetation and soil types, roots of vegetations can be distributed only in the upper layer or in all soil layers. The vegetation types are identified by their LAI, canopy resistance, and relative fraction of roots in each of the two soil layers. Infiltration, soil moisture movement between different soil layers, runoff, as well as the energy variables in each grid are calculated separately on the basis of different vegetation types. Meteorological variables, primarily precipitation, maximum temperature, minimum temperature, and wind speed, make up the climate forcings of the VIC model.

Water balance simulation in the VIC model mainly considers ET, surface runoff, and baseflow at a time step of hour or a day. Three types of ET, including ET from the canopy layer of each vegetation class, transpiration from each of the vegetation classes, and ET from bare soil, are also considered in the model. The ET from each vegetation type is characterized by potential ET, aerodynamic resistance to water transfer, and architectural resistance (Liang et al., 1994, 1996a,b), whereas ET from bare soil is characterized by terrain, infiltration and soil property. Total ET at each grid cell is computed as the sum of the canopy, vegetation, and bare soil components, weighted by the respective surface cover area fractions (Liang et al., 1994).

As mentioned above, VIC adopts a spatially varying infiltration curve to solve the infiltration in surface runoff calculation, and the curve is used to represent subgrid variability in soil properties and topographic effects. The spatial distribution of the infiltration capacity is given by

$$i = i_m[1 - (1 - A)^{1/b_i}] \quad (1)$$

where i and i_m are the infiltration capacity and maximum infiltration capacity, respectively; A denotes the fraction of an area where the infiltration capacity is less than i; and b_i is the infiltration shape parameter.

Generally, the physically based VIC model is developed to simulate the water and energy balances for large-scale applications (Cherkauer and Lettenmaier, 1999; Hamlet and Lettenmaier, 2007; Liu et al., 2010; Matheussen et al., 2000). However, models for small and medium-sized basins have been applied in recent years (Liu et al., 2011; Zhang et al., 2009; Zhou et al., 2004). For example, Zhou et al. (2004) successfully used the VIC model to simulate the water fluxes of the Baohe River Basin, which has a

drainage area of 2500 km^2. Zhang et al. (2009) applied the VIC model and the Soil and Water Assessment Tool to the Bailian River watershed to discuss the adaptability of these models in the flow simulation of the mid-small valley. Their results showed minimal simulation difference between the two models.

Moreover, at a minimum, the VIC model can be driven by gridded precipitation, temperature, and wind time series, all of which are readily available from the Meteorological Information Center, China Meteorological Administration. Therefore, the model was implemented to assess the historical and potential hydrologic responses with a grid cell resolution of 1/32° latitude and longitude in the DYP watershed.

2.2. Land-use change model

The CLUE-S (conversion of land-use and its effects) model developed by the University of Wageningen in the Netherlands was employed to simulate land-use/cover change using empirically quantified relationships between land-use and its driving factors. This approach was used in combination with dynamic modeling. The model is sub-divided into two modules: a non-spatial demand module and a spatially explicit allocation procedure. The non-spatial module calculates the area of change demanded for all land-use types at the aggregate level, and the allocation module is used to allocate these demands to different locations within the study area using a raster-based system (Verburg et al., 2002).

Usually, an empirical analysis unravels the relationships between the spatial distribution of land-use and a series of factors that are land-use drivers and constraints. The relationships between land use and its driving factors are evaluated using stepwise logistic regression, which can indicate the probability of a certain grid cell to be devoted to a land-use type given a set of driving factors described as follows:

$$\mathrm{Log}(P_i/1-P_i) = \beta_0 + \beta_1 X_{1,i} + \beta_2 X_{2,i} \ldots + \beta_n X_{n,i} \quad (2)$$

where P_i is the probability of a grid cell to be used for the considered land-use type; $X_{n,i}$ are driving factors; and β_i represents the coefficient of each driving factor in the logistic model (Verburg et al., 2002).

Then, the restricted area and land-use decision rules that determine the spatio-temporal dynamics of the simulation were specified for the study region. These rules include land-use conversion elasticities and land-use transition sequences. Conversion elasticities are related to the reversibility of land-use changes, while the land-use transition sequences are specified in a land-use conversion matrix (Chen et al., 2009). On the basis of the regression results, a probability map can be calculated for each land-use type. A new probability map is calculated every year using updated values for the driving factors that are projected to change with time (Verburg et al., 2002).

Finally, land-use change is allocated using an iterative procedure based on the probability maps, the decision rules in combination with the actual land-use map, and the demand for the different land-use types. The first step includes the determination of all grid cells that are allowed to change. Grid cells that are either part of a protected area or under a land-use type that is not allowed to change are excluded from further calculation. Next, for each grid cell, the total probability is calculated for each of the land-use types according to the value of initial probability, the iteration variable, and the relative elasticity for change specified in the decision rules. Third, the total allocated area for each land use is now compared with the demand. For land-use types where the allocated area is smaller than the demanded area, the value of the iteration variable is increased and vice versa. The above-mentioned procedures are repeated until the demands are correctly allocated. When allocation equals demand, the final map is saved, and the calculations can continue for the next yearly time step (Verburg et al., 2002).

2.3. Description of the watershed

The DYP watershed, located in the middle of Sichuan Province, belongs to upstream Yangtze River Basin (Fig. 1). As a major upper sub-basin of the Qingyi River, this watershed is mountainous and heavily forested. The total area above the Duoyingping gauge station is 859,946 ha, with geographical ranges of 29.38–30.99°N and 102.18–103.24°E. The DYP watershed has a wide range of elevation, from 588 m at its lowest point to 5298 m at its highest peak. This domain belongs to the subtropical zone with a humid monsoon climate, and annual average temperature ranges from 15 to 18 °C. Annual precipitation varies between 730 and 1720 mm, with an average of 1200 mm. Influenced by geographical position and monsoon circulation, dry and wet seasons are clearly defined, and more than 60% of precipitation occurs during the wet season from July to September.

Precipitation varies from place to place and generally increases from the northwest to the southeast. Rainstorm areas cover most of the watershed. According to the soil database developed by Reynolds et al. (1999), about 77% clay-loam and 23% loam comprise the soil of the total area. Dominant land-use patterns are forest, shrubland, and grassland, which account for 88.6% of the entire watershed in 2000, whereas urban areas and bare land account for only approximately 1%. The main tree species are spruce and hemlock, which are mixed with a quantity of alpine pine and Chinese pine. In this study, the watershed was divided into 10 sub-watersheds (Fig. 1) using selected digital elevation model (DEM) data as bases for later use.

2.4. Data preparation

2.4.1. DEM data

A DEM with a spatial resolution of 3 arc-second (approximately 90 m) was obtained from the Shuttle Radar Topography Mission (SRTM) website (http://srtm.csi.cgiar.org). The SRTM data, measured by NASA and the National Imagery and Mapping Agency, are available at the range of 60°N–60°S with a geodetic datum of WGS84. The data are currently being distributed by NASA/USGS. In this study, the downloaded SRTM data were used as a base map for hydrologic modeling.

2.4.2. Soil data

The spatial soil data, with a resolution of 5 min (approximate 10 km), were obtained from the United States Department of Agriculture (USDA) Agricultural Research Service, and were published by the NOAA National Geophysical Data Center, Boulder, Co (Reynolds et al., 1999). On the basis of the relative proportions of sand, silt, and clay particles in a soil material that has a particle size of less than 2 mm (diameter), soil texture classes were reclassified into 12 types in accordance with the USDA soil classification system. Soil hydraulic properties, including field capacity, wilting point, saturated hydraulic conductivity, porosity, bulk density, and slope of retention curve, were estimated based on soil texture classes, sand, clay, and silt content following Cosby et al. (1984) and Su and Xie (2003).

2.4.3. Land-use data

Land-use data for 1980, 1995, and 2000 were obtained from the Environmental and Ecological Science Data Center for West China, National Natural Science Foundation of China (http://westdc.westgis.ac.cn). The dataset, with a spatial resolution of 1 km, was created by Chinese Academy of Sciences (CAS) in accordance with

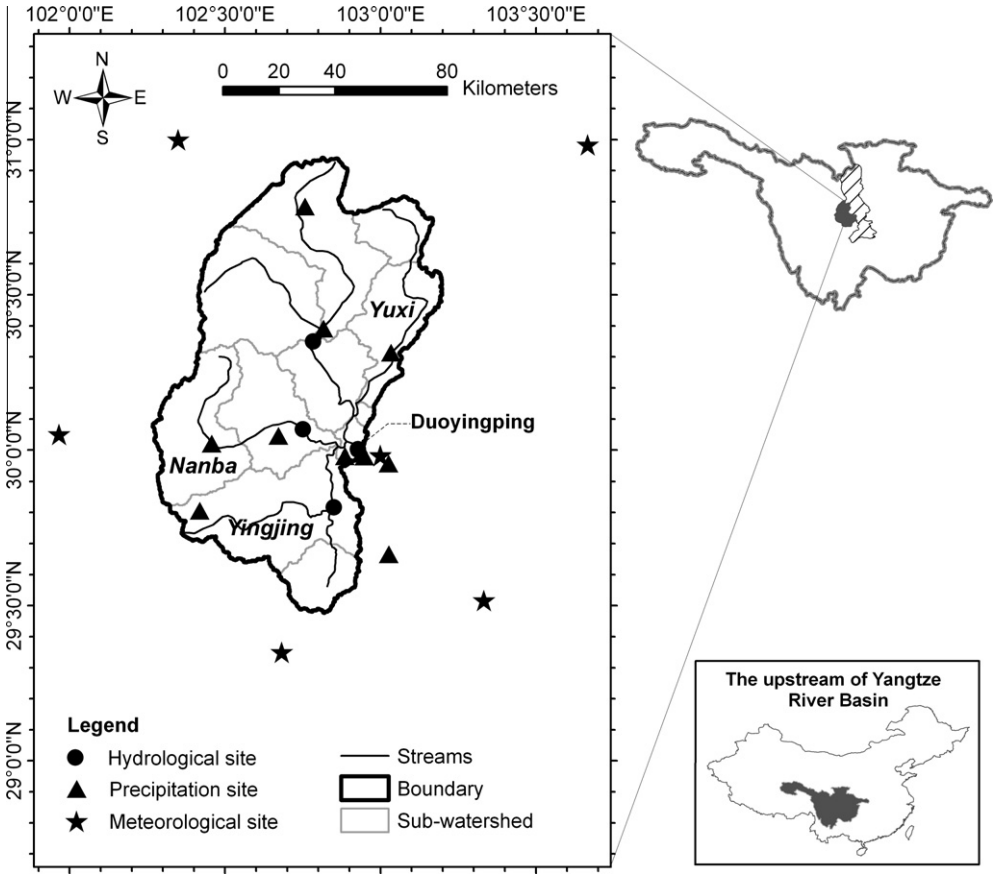

Fig. 1. Location of the Duoyingping watershed.

the land-use maps in the same period on a scale of 1:100,000. The current study is focused primarily on hydrologic responses to historical and potential land-cover change; thus, the coverage areas under water, settlement, and bare land accounting for less than 1.5% of the study domain were disregarded in hydrologic modeling and were all considered as non-forest in the land-use scenario. Therefore, land-cover types derived from the resource and environment classification of the CAS were categorized into less specific types (Table 1) commonly used by the VIC model: forest, shrubland, grassland, and cropland.

The reclassified land-cover data for all the three periods were first used to analyze the historical dynamics of land-use, and then used to generate potential land-cover scenarios. Finally, the data were incorporated as input into the VIC model (details are discussed later in the paper).

For each vegetation type, the vegetation parameters, such as monthly LAI, ALB, architectural resistance, minimum stomata resistance, roughness length, fraction of root depth, and zero-plane displacement, were derived from the Land Data Assimilation System (LDAS) dataset, as well as from Su and Xie (2003). The value ranges for LAI and ALB are summarized in Table 1.

Table 1
Transformation of CAS land-cover types to VIC model land-cover types.

Vegetation class of CAS	Vegetation class of VIC	LAI	ALB
Paddy field Dry land	Cropland	0.02–5.00	0.10
Forest land Open forest land Other forest land	Forest	1.52–5.00	0.18
Shrubbery High-coverage grassland	Shrubland	2.20–3.85	0.19
Moderate-coverage grassland Low-coverage grassland	Grassland	2.20–3.85	0.20

Note: LAI, Leaf Area Index; ALB, albedo.

2.4.4. Hydro-meteorological data

The model forcing data, which are standard for VIC, include precipitation (mm), maximum and minimum air temperature (C°) (T_{max} and T_{min}), and mean wind speed (m/s). Daily climate data series from six sites of the National Meteorological Observatory (NMO) located around the DYP watershed were collected over the period 1980–2005. These data provided by the China Meteorological Administration include precipitation, T_{max}, T_{min}, wind speed, and humidity. In addition, daily observed precipitation and streamflow series from 10 precipitation stations and four hydrological stations located in the DYP watershed during the period 1984–1987 were obtained from the Hydrological Yearbook of the Min-tuo River. Moreover, another observed daily streamflow at the Duoyingping hydrological station during several non-consecutive periods were also collected from the local Bureau of Hydrology. Data periods were June 1998 to September 1998, May to November in 1999–2001, and April to November in 2002–2004. All the forcing data series, including precipitation, mean wind speed, T_{max}, and T_{min}, were interpolated to the 821 divided grid cells using the inverse distance interpolation method. Fig. 1 shows the location of these stations in the watershed.

Given that this study focused only on the effect of land-cover change on hydrology, effects of climate change required minimization. On the basis of the Mann–Kendall trend test (Mann, 1945; Kendall, 1975) on precipitation, T_{max}, T_{min}, and mean wind speed at the six Meteorological Observatory sites, it was found that only

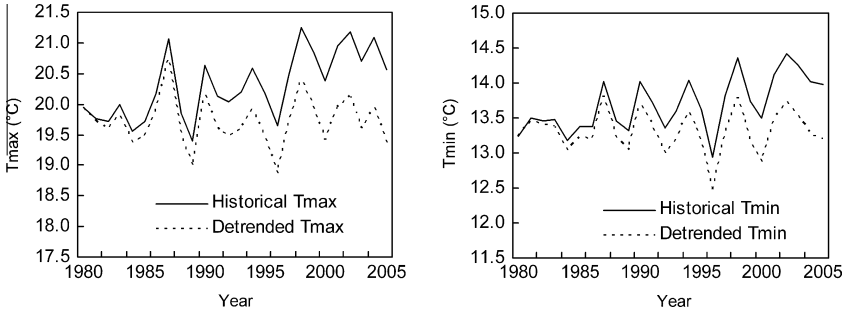

Fig. 2. Historical and detrended annual T_{max} and T_{min} series on cell node 29.9923°N, 102.9355°E.

T_{max} and T_{min} exhibited a statistically significant increasing trend over 1980–2005. Therefore, this long-term increasing trend was eliminated, whereas the time series elements of the daily variations within the month were retained using the method described by Hamlet and Lettenmaier (2007). The historical and detrended T_{max} and T_{min} series on a single cell (29.9923°N, 102.9355°E) are plotted in Fig. 2.

The VIC model was used to examine the effect of vegetation change on the hydrology of the study region using the detrended 26 years (1980–2005) of meteorological data for both historical and potential land-cover scenarios.

2.5. Model calibration and verification

Monthly values of simulated streamflow were compared with observations to calibrate the VIC model. The dataset was divided into two parts: a calibration period (1984–1987) and a verification period (1998–2004). According to Liang et al. (1994) and Matheussen et al. (2000), seven soil parameters, including b_i, D_s, D_m, W_s, d_1, d_2, and d_3 in the VIC-3L model should be adjusted to improve the agreement between simulations and observations. Specifically, D_m (mm/day) and D_s represent the maximum velocity of baseflow and the fraction of D_m where non-linear baseflow begins respectively; W_s indicates the fraction of the maximum soil moisture where non-linear baseflow occurs; d_1, d_2 and d_3 (m) denote the soil depth of layers 1, 2 and 3 respectively; and b_i is the infiltration shape parameter. In the current work, calibration was conducted by trial and error until satisfactory results were obtained. Once the soil parameters were accepted after calibration, they were evaluated against observed streamflow for the entire period and used for various land-cover scenarios in the study region.

The first criterion we used to evaluate the goodness of fit between observations and simulations is the Nash–Sutcliffe efficiency (NSE) coefficient (Nash and Sutcliffe, 1970). The value of the NSE coefficient is always expected to approach 1 for a simulation of the observed value series to be regarded as good; an indicating fraction of the variances in the observed values is explained by the model. The second efficiency criterion used to evaluate the performance of the model is the relative error (RE), which represents a systematic water balance error. The value of RE is expected to be close to 0 for good simulation. NSE and RE are defined as

$$\mathrm{NSE} = 1 - \frac{\sum_{i=1}^{n}(Q_{obs,i} - Q_{sim,i})^2}{\sum_{i=1}^{n}(Q_{obs,i} - \overline{Q}_{obs})^2} \quad (3)$$

$$\mathrm{RE} = (\overline{Q}_{sim} - \overline{Q}_{obs})/\overline{Q}_{obs} \quad (4)$$

where $Q_{obs,i}$ and $Q_{sim,i}$ are the observed and simulated streamflows, respectively; $\overline{Q}_{obs}$ and $\overline{Q}_{sim}$ represent the mean values of the observed and simulated streamflows, respectively; and n is the length of time series.

The simulation results for the Duoyingping, Baoxing, Tianquan, and Yingjing hydrological stations are illustrated in Fig. 3. Overall, all observed monthly values are consistent with the simulated values. During the calibration period, the NSE values for the model were 0.862, 0.777, and 0.831, and the REs were −13.2%, −17.7% and −14.1% at the Duoyingping, Tianquan, and Yingjing stations, respectively. The Baoxing station, which controlled the

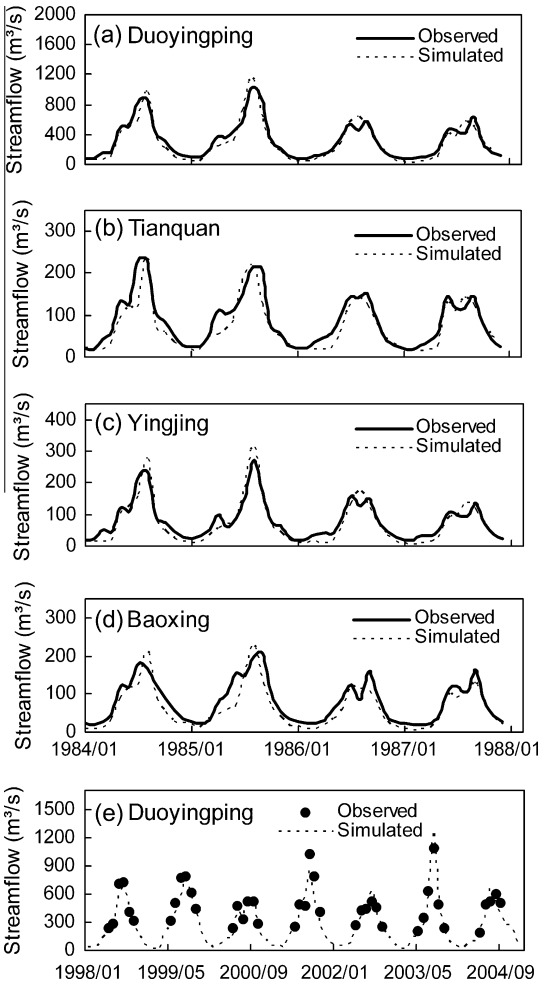

Fig. 3. Monthly hydrographs for calibration and verification: a–d describe hydrographs at the Duoyingping, Tianquan, Yingjing, and Baoxing Station during the calibration period, respectively; e describes hydrograph at the Duoyingping Station during the verification period.

northwestern watershed, registered scarce precipitation observations that resulted in a lower NSE value and a larger RE of 0.719 and −23.8%.

Because no observed streamflows are available after 1990s at the Baoxing, Tianquan, and Yingjing stations, verification was conducted only at the Duoyingping station. The verification was based on several non-consecutive observations during the wet season from 1998 to 2004. The hydrograph shape indicates good agreement in the verification period, with NSE = 0.752 and RE = −10.9%, reflecting acceptable model performance within the studied watershed. Therefore, model parameters were used for all the simulation scenarios in the study.

3. Results and discussion

3.1. Historical land-cover change between 1980 and 2000

Dynamics in historical land-cover were examined on the basis of reclassified land-use/cover maps for 1980, 1995, and 2000 (Fig. 4). The areas under different land-use types and the changes they have undergone are given in Table 2.

In general, most areas in the DYP watershed were occupied by forest, shrubland, grassland, and cropland (accounting for more than 98% of the total area) in 1980–2000. In 1980, most of the area was occupied by shrubland and grassland (72.2%), followed by forest (16.6%) and cropland (10.5%). By 1995 and 2000, the largest proportion of the watershed remained under shrubland and grassland (71.2% and 70.1%, respectively), followed by forest and cropland. Remarkable changes in vegetation cover occurred in the southwestern and northeastern areas of the watershed, whereas land-cover change was relatively small in other regions.

From 1980 to 1995, the forest, shrubland, and non-forest areas increased, whereas the grassland and cropland areas decreased. For all vegetation types, the largest increase was observed in the forest area (increased by 12.7%), followed by shrubland, which increased by 5.1%, mainly at the expense of grassland. The largest decrease occurred in cropland (decreased by 14.6%), followed by grassland, which decreased by 8.2% at a rate of 1586.5 ha/yr.

From 1995 to 2000, grassland coverage increased by 4.1% at an increase rate of 2180.4 ha/yr. The cropland area increased by 18.4% at an increase rate of 2792.4 ha/yr. Cropland increase was caused primarily by the degradation and deforestation of forest and shrubland during this period. By contrast, the forest, shrubland, and non-forest areas decreased. The decrease rates were 4045.8 ha/yr for shrubland (6.0% decrease) and 478.4 ha/yr for forest (1.5% decrease).

Overall, Fig. 4 and Table 2 show that the most substantial changes in land-use/cover over the past decades were concentrated in the forest, shrubland, grassland, and cropland areas. Two-way conversion (mutual conversion) among various vegetation types was the main characteristic of these dynamics. For example, between 1980 and 1995, a large number of shrubland regions in southern Yingjing were reforested, but in western Tianquan, more than 50% of the forest was diverted to shrubland over the same period. Interestingly, a completely opposite trend

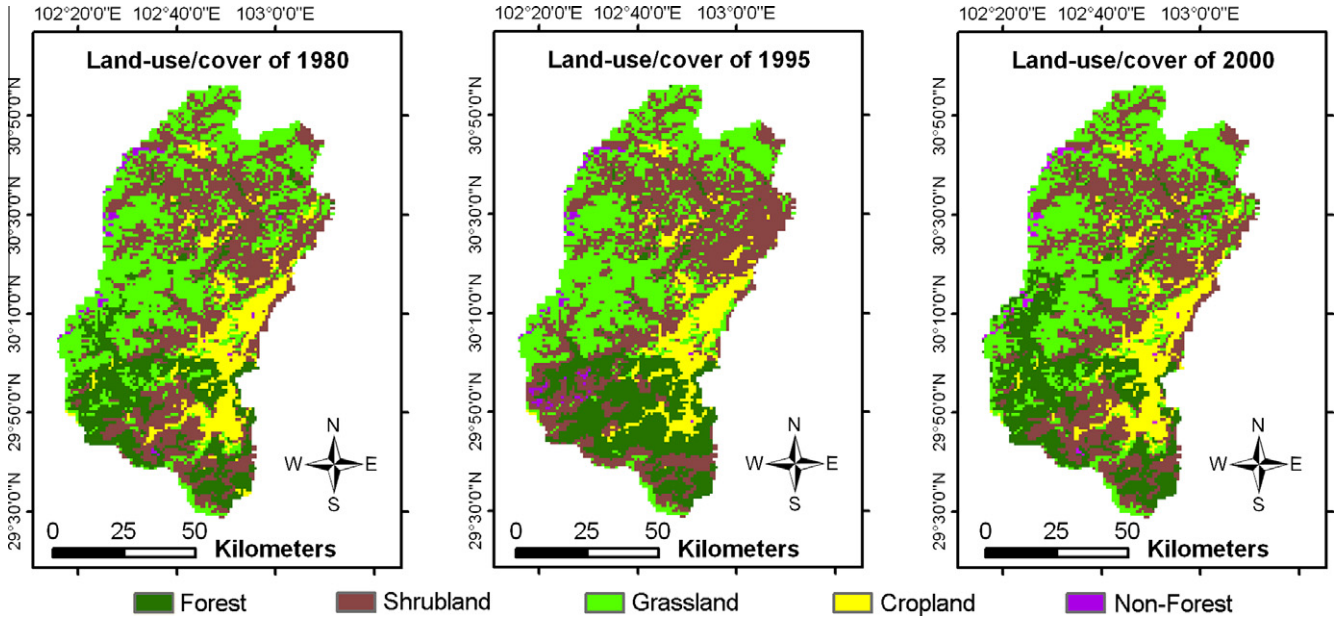

Fig. 4. Land-use/cover maps for 1980, 1995, and 2000 of the DYP watershed.

Table 2
Land-use/cover change between 1980 and 2000 in the DYP watershed.

Land-use/cover	Area in 1980		Area in 1995		Area in 2000		Change (%)	
	10^4 ha	% of total	10^4 ha	% of total	10^4 ha	% of total	1995–1980	2000–1995
Forest	14.1	16.6	15.9	18.7	15.7	18.5	12.7	−1.5
Shrubland	32.0	37.8	33.7	39.7	31.6	37.3	5.1	−6.0
Grassland	29.2	34.4	26.8	31.5	27.9	32.8	−8.2	4.1
Cropland	8.9	10.5	7.6	8.9	9.0	10.6	−14.6	18.4
Non-forest	0.7	0.8	0.9	1.1	0.7	0.8	40.3	−23.9
Total	84.9	100.0	84.9	100.0	84.9	100.0	–	–

was observed when changes in land-use/cover were compared over the two periods (1980–1995 and 1995–2000).

These land transformations can be attributed to the government reforestation policy implemented since the 1980s. This policy which resulted in an increase in forest and shrubland areas and a decrease in grassland areas between 1980 and 1995. However, the deficient water-storage capacity of young forest and shrubland, together with the over-logging of arbor forest caused by a high rate of population growth and rapid economic development, led to severe soil and water loss. This is why forest areas decreased sharply and grassland areas expanded widely after 1995. Additionally, the Grain-for-Green Programme was implemented beginning 1999 to prevent soil erosion and improve the eco-environment, which has also affected the process of land-cover change and may play an important role in the future.

3.2. Simulation of potential land-cover scenarios

3.2.1. CLUE-S model calibration

The CLUE-S model was calibrated on the basis of the collected 1980, 1995 land-use maps. The annual land-use demands in these periods were obtained using a linear interpolation method. The natural and socioeconomic factors that drive land-use change in the DYP watershed include elevation, slope, aspect, compound topographic index (CTI), stream power index (SPI), distances to city, village, road, and river, population density, GDP, annual rainfall, and soil type. All of the driving factors and land-use data were converted into a grid with a resolution of 1 km. The nature reserves in the DYP watershed were considered restricted areas that could not be changed over the simulation period. The relative operating characteristic (ROC) was used to assess the goodness of fit of a logistic regression model.

We performed forward stepwise logistic regression and ROC analysis using the SPSS for Windows. The estimated coefficients and relative ROC values for the main land-use types are listed in Table 3. The ROC values from the logistic model ranged from 0.779 to 0.936, indicating that the model is capable of representing the spatial dynamics of land-use/cover patterns.

The results of the logistic models, land-use demands, and land-use/cover elasticities were applied to simulate the land-cover change for 1980–1995. The initial parameters of land use conversion elasticities were obtained from Verburg et al. (2002). On the basis of the characteristics of land-use change in the watershed, conversion elasticities were adjusted by trial and error to minimize errors. Compared with the results from the land-use/cover map of 1995, the best-fit simulation output has a Kappa accuracy of 81.6% (the ratio between the number of cells with correct simulation and the total number of cells), indicating that the chosen driving factors can accurately explain the land-use/cover change. Therefore, model performance is acceptable within the study domain and can simulate land-use/cover scenarios.

Table 3
Driving factors and the coefficients of the regression results for each land-cover type.

Divers	Forest	Shrubland	Grassland	Cropland
Elevation	−0.0016	0.0003	0.0012	−0.0019
CTI	−0.2614	−0.1079	0.1329	0.3321
SPI	0.1471	0.1207	−0.0948	−0.3626
Slope	−0.0627	−0.0014	0.0297	0.0893
Aspect	0.0007	−0.0003	−0.0013	0.0017
Distance to river	0.00007	−0.0001	0.00006	−0.0003
Distance to city	0.0001	−0.00009	–	−0.00007
Distance to village	−0.00009	–	0.00006	−0.0003
Distance to road	−0.00005	–	–	–
Rainfall	−0.0014	−0.0009	0.0037	−0.0020
Population density	−0.0050	−0.0005	−0.0011	0.0040
GDP	−0.00006	–	–	0.0002
Leached soil	0.9237	−0.6276	−0.0227	−0.4835
Primitive soil	0.5612	−0.8285	0.0756	0.0550
Artificial soil	0.2967	−0.4484	−0.9790	0.3084
Alpine soil	0.5730	−1.0326	0.0404	−12.1340
Constant	6.3931	0.4595	−10.2364	3.6860
ROC	0.848	0.779	0.821	0.936

Note: "–" denotes nonsignificance at 0.05 level.

3.2.2. Generation of potential land-cover scenarios

Using the calibrated parameters as bases, we simulated two kinds of future land-cover scenarios using the CLUE-S model for 2000–2030 at a yearly time step based on different land-use demands. In scenario 1, the change trend of land-cover in the closed period 1995–2000 was constant, and free conversion was allowed to calculate the land-use demands using the Markov process (Muller and Middleton, 1994). The land-use demands were characterized by an increase in cropland and grassland, along with considerable decreases in shrubland and a slight decrease in forest. In scenario 2, under the national policies *Grain-for-Green and Soil Erosion Control* implemented in 1999, the annual decrease rate of cropland was determined as 1.31% following Ma (2004) and Xiao et al. (2008), whereas the area of forest increased by about 4298.1 ha/yr on the basis of the statistical data of local forest department. Non-forest could not converted into other land-cover types and vice versa. The different demands for vegetation cover under the two scenarios are plotted in Fig. 5.

For easy comparison, the final land-cover scenario for 2030 was selected as the input data to assess the cumulative effect on future hydrologic conditions. The simulation results for 2030 under both scenarios are shown in Fig. 6.

3.3. Setting of historical and potential land-cover scenarios

On the basis of the investigation on historical land-cover change, the land-use scenarios of 1995 and 2000 were selected to examine the hydrologic effect of historical deforestation during this period. In addition, the two future land-cover scenarios for

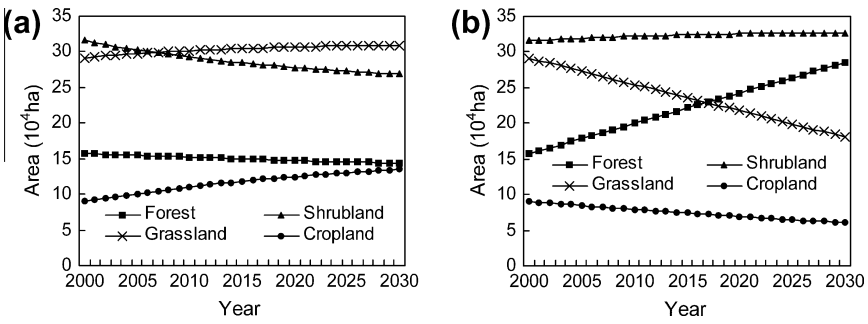

Fig. 5. Potential land-cover demands during 2000–2030: (a) under scenario 1, (b) under scenario 2.

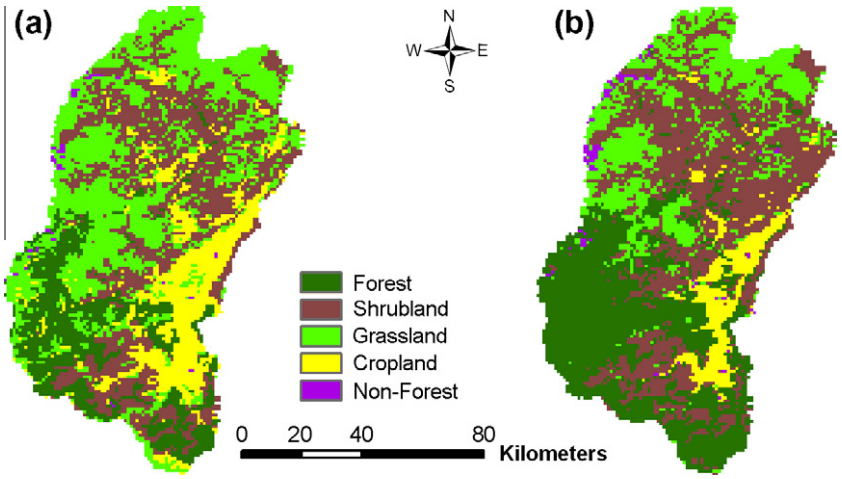

Fig. 6. Potential land-use/cover scenarios for 2030: (a) based on demands of scenario 1, (b) based on demands of scenario 2.

2030 generated by the CLUE-S model were applied to assess the effect of potential land-cover change in future hydrologic processes using 2000 as the baseline. Overall, the effect of the land-cover change on hydrology was quantified by comparing the VIC output of the four selected scenarios as follows:

H1: 1995 land-cover
H2: 2000 land-cover
F1: 2030 land-cover under historical change trend
F2: 2030 land-cover under the national policies *Grain-for-Green and Soil Erosion Control*

Therefore, the difference between the hydrologic results for H1 and H2 (Scenario A: H2–H1) indicate the effect of historical land-cover change between 1995 and 2000 on hydrologic processes, whereas the hydrologic differences for F1–H2 (Scenario B1) and F2–H2 (Scenario B2) represent the effect of potential land-cover change on hydrology under different policies on land-use demand.

3.4. Effect of historical and potential land-cover change on hydrologic processes

3.4.1. Effect on annual hydrologic components

Subsequently, the VIC model was applied in the study domain using the detrended climate data series over the period 1980–2005 (as mentioned in the "Data preparation" section) for both historical and future land-cover scenarios. The spatial differences in runoff, ET, and soil moisture under scenarios A (H2–H1), B1 (F1–H2), and B2 (F2–H2) are plotted in Fig. 7. These differences can be related directly to the changes in land-cover patterns shown in Fig. 4 and Fig. 6.

Effect of historical land-cover change. Between 1995 and 2000, annual runoff decreased from 8.3 to 100.1 mm/yr (1.0–12.3%) in western Nanba; this decrease was induced by reforestation in the shrubland and grassland areas. However, conversion from forest to shrubland and cropland in southern Yingjing led to a 3.0–105.5 mm/yr (0.2–10.5%) net increase in runoff. The replacement of shrubland with grassland also resulted in increases in runoff of approximately 7.7–41.3 mm/yr (0.6–3.2%) in northeastern Yuxi. The changes in ET exhibited a magnitude opposite to the changes in runoff as expected, and reforestation yielded a 8.5–100.3 mm/yr (2.3–27.4%) increase in annual ET in western Nanba. ET decreased from 3.0 to 105.7 mm/yr (0.8–22.3%) and 7.6 to 41.1 mm/yr (2.1–11.3%) in southern Yingjing and northeastern Yuxi, respectively, because of the destruction of forest and shrubland. The change patterns of soil moisture were similar to those of runoff, but smaller in magnitude. For instance, soil moisture reduced by 0.7–7.4 mm/yr (0.5–5.3%) in western Nanba, but increased from 0.1 to 7.0 mm/yr (0.1–5.1%) and 0.3 to 2.0 mm/yr (0.2–1.4%) in Yingjing and Yuxi, respectively, between 1995 and 2000.

Effect of potential land-cover change. In scenario B1 (Fig. 7b), changes in hydrologic components mainly occurred where cropland expanded at the expense of shrubland and where forest

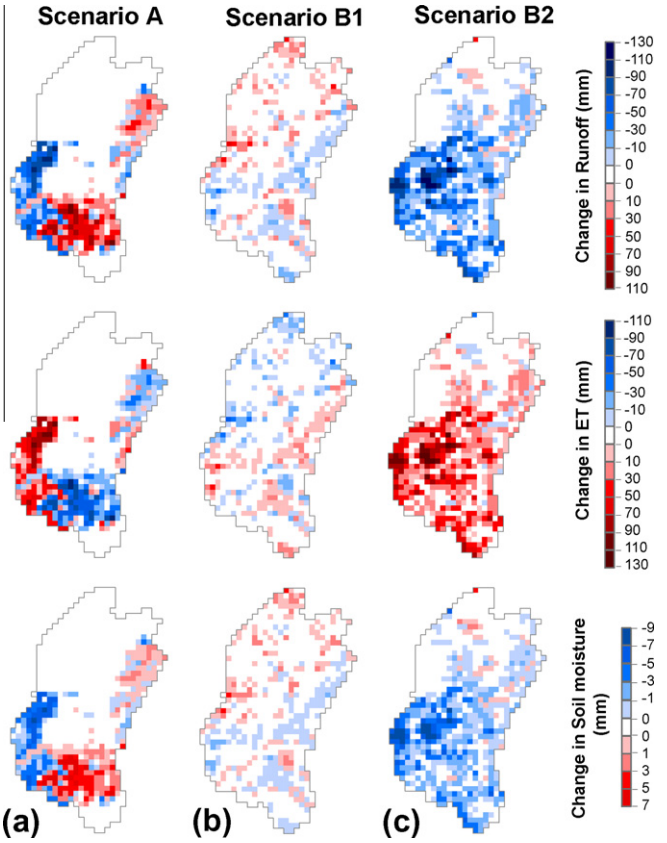

Fig. 7. Spatial differences in annual hydrologic components due to land-cover change: (a) Scenario A represents hydrologic effect of historical land-cover change, (b) Scenario B1 and (c) Scenario B2 represent hydrologic effect of different potential land-cover changes, respectively.

and shrubland have been converted to grassland. For instance, in the northwestern and southeastern areas of the watershed where forest has been converted to cropland, annual runoff increased from 3.6 to 26.2 mm/yr (1.1–3.3%), ET decreased from 3.2 to 28.1 mm/yr (1.0–6.6%), and soil moisture increased slightly by 0.7–2.0 mm/yr (0.6–1.5%). Similarly, the replacement of shrubland with grassland in the northern and western areas of the watershed resulted in increases in runoff and soil moisture from 3.7 to 33.3 mm/yr (0.3–8.7%) and 0.2 to 1.6 mm/yr (0.1–1.0%), respectively. By contrast, ET exhibited a reduction of around 3.7–33.0 mm/yr (1.2–9.2%) in these regions. In the eastern and partial central parts of the watershed, a large area of shrubland was converted to cropland. These modifications led to increases in ET by 0.8–16.4 mm/yr (0.2–4.4%), while runoff and soil moisture decreased from 0.7 to 15.5 (0.1–1.3%) and 0.1 to 1.2 mm/yr (less than 0.1%), respectively.

The largest changes in hydrologic components resulted from forest conversion to grassland and replacement of shrubland with forest. For instance, forest conversion to grassland yielded a 58.6 mm/yr increase in runoff and a 58.7 mm/yr reduction in ET in northwestern Nanba, whereas shrubland conversion to forest generated 33.1 mm/yr less runoff and 34.2 mm/yr more ET in southwestern Nanba.

In scenario B2 (Fig. 7c), the major land-cover changes were caused by forest and shrubland expansion from grassland and cropland. More than 60% of the watershed exhibited hydrologic alteration because of the dynamics in vegetation types. ET experienced net increases of 6.2–128.4 mm/yr (1.5–36.7%), annul runoff decreased from 6.3 to 128.0 mm/yr (0.5–16.2%), and soil moisture also represented a reduction of around 0.4–8.2 mm/yr (0.3–6.0%) in most areas of the watershed because of afforestation. The grassland conversion to forest in the central and part of the southern parts of the watershed contributed the most to these hydrologic changes, with an average reduction of 66.4 mm/yr (7%) and 4.5 mm/yr (3.2%) in runoff and soil moisture, respectively, and an average increase of 66.5 mm/yr (18.3%) in annual ET. Under the *Grain-for-Green and Soil Erosion Control* policies, a large portion of the cropland area was converted to forest in the downstream part of the watershed, thereby causing decreases in runoff and soil moisture of 30.0 mm/yr (2.2%) and 1.8 mm/yr (1.2%), respectively, but increases in ET of 28.0 mm/yr (7%) on average.

Moreover, the replacement of grassland with shrubland in the northern part of the watershed also played a role in the reduction of annual runoff and soil moisture, as well as in the increases in annual ET. Conversely, changes from cropland to shrubland in part of the northern area of the watershed yielded a 1.5–10.2 mm/yr (0.4–2.7%) net reduction in ET and slight increases of 1.6–10.0 mm/yr (0.1–0.7%) and 0.1–0.8 mm/yr (less than 0.5%) in runoff and soil moisture, respectively.

The interpretation of these hydrologic alterations may mainly stem from changes in LAI values between different land-cover types. In general, a forest can intercept and exhaust more water through ET than can other vegetation types because it has the highest LAI, which reduces surface water volume and soil moisture. Although the canopy height and monthly LAI of shrubland were larger than those of cropland during the dry season, cropland lost more moisture to the atmosphere compared with shrubland because the largest amount of rainfall occurred during the wet season, when cropland had the largest LAI in the DYP watershed. In addition, shrubland and grassland had similar LAIs for all

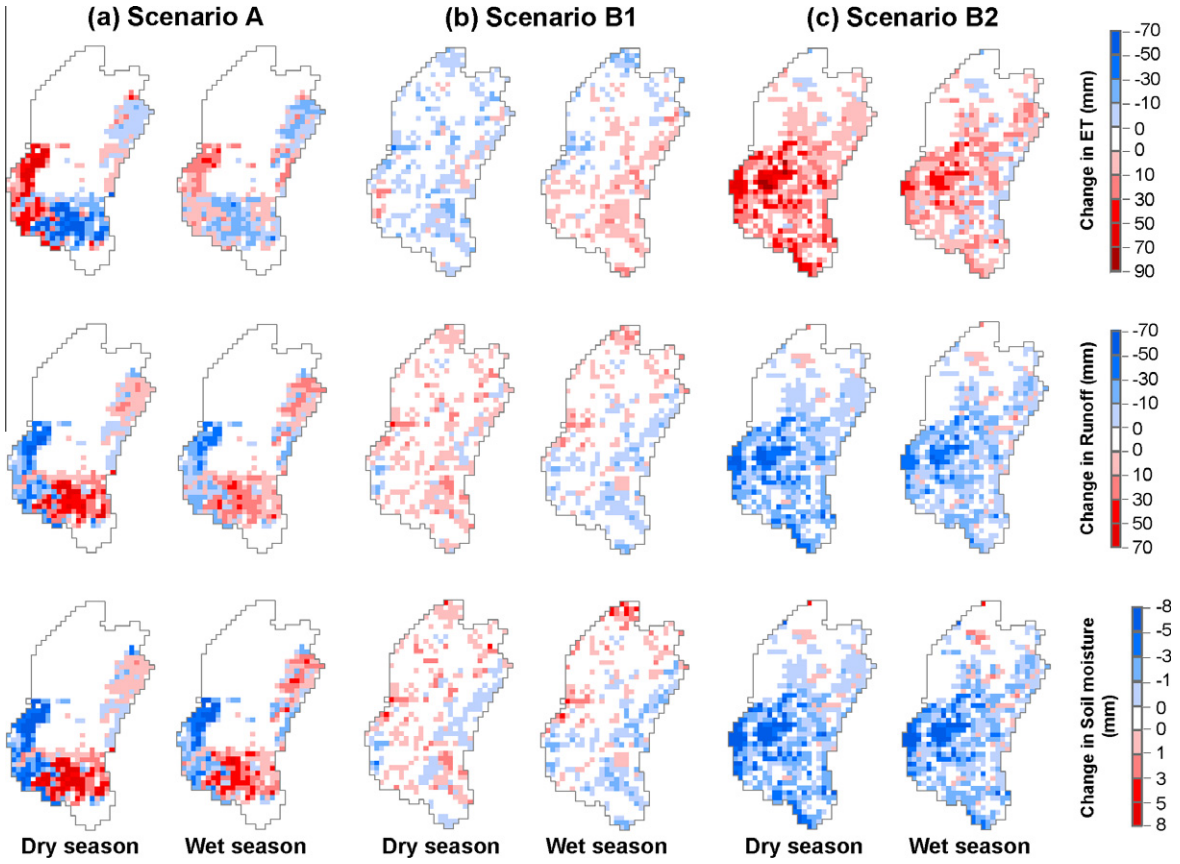

Fig. 8. Spatial differences in seasonal hydrologic components due to land-cover change: (a) Scenario A represents hydrologic effect of historical land-cover change, (b) Scenario B1 and (c) Scenario B2 represent hydrologic effect of different potential land-cover changes, respectively.

months, which is why changes in hydrologic components were negligible where conversion between the two kinds of vegetation occurred.

Overall, the changes in ET and runoff were more sensitive to both historical and potential land-cover change, particularly in ET. This may be explained by the easy saturation of soil moisture (regarded as a hydrologic intermediate variable) by heavy rainfall and frequent relieving by ET and runoff. However, because of the different patterns of land-cover change scenarios, the effects on hydrology constantly change from case to case. In scenario A, mutual conversions between several vegetation classes counteracted the hydrologic effect of land-cover change for the entire watershed. With respect to potential scenarios (B1 and B2), dramatic afforestation affected hydrologic processes to a greater degree in scenario B2 compared with a relatively small cropland expansion in scenario B1.

3.4.2. Effect on seasonal hydrologic components

For better understanding, the annual average seasonal hydrologic components, including ET, runoff, and soil moisture in the different land-cover scenarios were compared in comprehensively exploring the spatial changes in hydrologic responses (Fig. 8). In scenario A (Fig. 8a), dry season (October–May) ET was enhanced from 7.1 to 67.2 mm/yr (4.5–43.8%) in western Nanba because of reforestation compared with increases from 1.4 to 29.5 mm/yr (0.7–13.6%) during the wet season (June–September). These results may be attributed to the heavy rains, which provide abundant water for ET that easily satisfy evaporative capacity during the wet season, whereas soil water content and groundwater play an important role in ET during the dry season. Soil moisture and groundwater can be significantly influenced by various land-cover types. Deforestation in southern Yingjing also reduced the dry season and wet season ET to 10.3–70.1 mm/yr (6.0–30.7%) and 4.0–35.6 mm/yr (1.8–14.4%), respectively.

In scenario B1 (Fig. 8b), the changes in ET induced by cropland expansion were relatively small, with an average reduction of 2.7 mm/yr (1.7%) during the dry season and an increase of 6.6 mm/yr (3.2%) during the wet season. These findings may be attributed to the constantly higher LAI of cropland during the wet season; the LAI exhausted more surface and underground water. Moreover, large-scale afforestation led to an increases of 4.6–77.4 mm/yr (2.7–51.4%) for dry season ET and 2.8–50.9 mm/yr (1.4–25.8%) for wet season ET in scenario B2 (Fig. 8c).

Changes in runoff for different seasons exhibited the reverse in terms of changes in ET as expected, but with less magnitude regardless of season. For instance, deforestation increased dry season runoff in southern Yingjing by 9.3–61.7 mm/yr (2.5–22.6%) and enhanced wet season runoff by 5.0–43.7 mm/yr (0.5–6.0%) in scenario A. On the other hand, afforestation in scenario B2 resulted in a reduction in dry season runoff from 4.1 to 69.7 mm/yr (1.1–22.8%) and 6.2 to 58.5 mm/yr (0.7–13.7%) in wet season runoff, accounting for half of the changes in ET. In addition, the conversion from forest and shrubland to cropland in scenario B1 increased dry season runoff by 2.2 mm/yr (1.0%) but decreased wet season runoff by 5.8 mm/yr (1.3%), resulting from the different monthly LAIs of cropland in different seasons.

Fig. 8 also illustrates spatial changes in soil moisture for the three scenarios. In general, these changes followed the same patterns as the annual average changes in soil moisture shown in Fig. 7. The variations in dry season ranged from −6.3% to 6.0%, −2.7% to 4.9%, and −6.5% to 5.0% for scenarios A, B1 and B2, respectively. During the wet season, the changes in soil moisture for the three scenarios varied from −3.9% to 3.8%, −1.6% to 4.1%, and −5.6% to 3.9%, respectively. Land-cover change played a minor role in seasonal changes in soil moisture, coincident with the description of annual average changes in the previous section.

4. Conclusion

This study adopted an approach that combines the CLUE-S and VIC models in assessing hydrologic responses to historical land-cover change, and investigating the potential effects of future land-cover change on hydrologic conditions. Detrended climate data over the period 1980–2005 in the DYP watershed were used.

Dynamics in historical land-cover scenarios in the last three decades were examined, revealing that the conversions among forest, shrubland and grassland dominated the land-cover change process in the study site. Specifically, land-cover change patterns were characterized mainly as reforestation and deforestation between 1980 and 2000. According to different land-use demand policies, two potential land-cover scenarios for 2030 were generated using the CLUE-S model, representing cropland expansion and large-scale afforestation.

Comparing the VIC results under the designed land-cover scenarios, the findings of this study can be summarized into three points. First, historical deforestation in southern Yingjing and northeastern Yuxi led to decreases in annual average ET, but increases in annual runoff and soil moisture, whereas reforestation in western Nanba exhibited the reverse. Annual ET exhibited a slight decrease because of cropland expansion in scenario B1, together with slight increases in runoff and soil moisture. However, dramatic afforestation in scenario B2 affected hydrologic processes to a greater degree with a large increase in annual ET and reduction in annual runoff and soil moisture.

Second, regardless of annual or seasonal factors, the changes in annual ET were most sensitive to both historical and potential land-cover change, followed by runoff. Soil moisture seems unaffected by land-cover change.

Finally, changes in hydrologic components caused by reforestation and deforestation during the dry season were more significant than those during the wet season, which were probably induced by the different evaporative modes.

Nevertheless, each step of this process is associated with a degree of uncertainty, which inevitably influences the direction and magnitude of the estimated results. For instance, data uncertainty caused by insufficient availability or quality and related space–time heterogeneity (Niehoff et al., 2002) may lead to inaccuracies in historical land-cover change investigation. Moreover, potential land-cover scenarios generated by the CLUE-S model are not intended to explicitly represent actual future situation because they represent only a few of all the possible land-cover realizations (Liuzzo et al., 2010). The assessment of the effects of land-cover change on hydrology is highly dependent on the hydrologic model, which presents numerous uncertainties stemming from the simplification of and the assumptions made in the structure. However, these problems are expected to be solved in future investigations using a rigorous uncertainty estimation method. Overall, the proposed approach serves as a useful tool for watershed land-use planning and water resource management.

Acknowledgements

This study has been supported by the Ministry of Water Resources public welfare Project (2011332003), National Natural Science Foundation (41030636) and National Science and Technology Support Programme (2008BAB29B08-02).

References

Bewket, W., Sterk, G., 2005. Dynamics in land cover and its effect on stream flow in the Chemoga watershed, Blue Nile basin, Ethiopia. Hydrol. Process. 19, 445–458.

Bowling, L.C., Storck, P., Lettenmaier, D.P., 2000. Hydrologic effects of logging in western Washington, United States. Water Resour. Res. 36 (11), 3223–3240.

Chen, Y., Xu, Y.P., Yin, Y.X., 2009. Impacts of land use change scenarios on storm-runoff generation in Xitiaoxi basin, China. Quatern. Int. 208, 121–128.
Cherkauer, K.A., Lettenmaier, D.P., 1999. Hydrologic effects of frozen soils in the upper Mississippi River basin. J. Geophys. Res. 104, 19599–19610.
Chu, H.J., Lin, Y.P., Huang, C.W., Hsu, C.Y., Chen, H.Y., 2010. Modelling the hydrologic effects of dynamic land-use change using a distributed hydrologic model and a spatial land-use allocation model. Hydrol. Process. 24, 2538–2554.
Cosby, B.J., Hornberger, G.M., Clapp, R.B., Ginn, T.R., 1984. A statistical exploration of the relationships of soil mixture characteristics to the physical properties of soils. Water Resour. Res. 20 (6), 682–690.
Fohrer, N., Haverkamp, S., Eckhardt, K., Frede, H., 2001. Hydrologic response to land use changes on the catchment scale. Phys. Chem. Earth, Part B 26 (7–8), 577–582.
Franchini, M., Pacciani, M., 1991. Comparative analysis of several conceptual rainfall–runoff models. J. Hydrol. 122, 161–219.
Germer, S., Neill, C., Krusche, A.V., Elsenbeer, H., 2010. Influence of land-use change on near-surface hydrological processes: undisturbed forest to pasture. J. Hydrol. 380, 473–480.
Ghaffair, G., Keesstra, S., Ghodousi, J., Ahmadi, H., 2010. SWAT-simulated hydrological impact of land-use change in the Zanjanrood Basin, Northwest Iran. Hydrol. Process. 24, 892–903.
Hamlet, A.F., Lettenmaier, D.P., 2007. Effects of 20th century warming and climate variability on flood risk in the western US. Water Resour. Res. 43, W06427. doi:10.1029/2006WR005099.
Hong, N.M., Chu, H.J., Lin, Y.P., 2010. Effects of land cover changes induced by large physical disturbances on hydrological responses in Central Taiwan. Environ. Monit. Assess. 166, 503–520.
Hundecha, Y., Brdossy, A., 2004. Modeling of the effect of land use changes on the runoff generation of a river basin through parameter regionalization of a watershed model. J. Hydrol. 292, 281–295.
Kendall, M.G., 1975. Rank Correlation Methods. Griffin, London.
Land cover dataset of China, Institute of Geographic Science and Natural Resources Research of the Chinese Academy of Sciences. <http://westdc.westgis.ac.cn>.
Legesse, D., Vallet-Coulomb, C., Gasse, F., 2003. Hydrological response of a catchment to climate and land use changes in Tropical Africa: case study South Central Ethiopia. J. Hydrol. 275, 67–85.
Liang, X., Lettenmaier, D.P., Wood, E.F., Burges, S.J., 1994. A simple hydrologically based model of land surface water and energy fluxes for general circulation models. J. Geophys. Res. 99, 14415–14428.
Liang, X., Wood, E.F., Lettenmaier, D.P., 1996a. Surface soil moisture parameterization of the VIC-2L model: evaluation and modification. Global Planet. Change 13, 195–206.
Liang, X., Lettenmaier, D.P., Wood, E.F., 1996b. One-dimensional statistical dynamic representation of subgrid spatial variability of precipitation in the two-layer variable infiltration capacity model. J. Geophys. Res. 101, 21403–21422.
Lin, Y.P., Hong, N.M., Wu, P.J., Lin, C.J., 2007. Modeling and assessing land-use and hydrological processes to future land-use and climate change scenarios in watershed land-use planning. Environ. Geol. 53, 623–634.
Lin, Y.P., Lin, Y.B., Wang, Y.T., Hong, N.M., 2008. Monitoring and predicting land-use changes and the hydrology of the urbanized Paochiao watershed in Taiwan using remote sensing data, urban growth models and a hydrological model. Sensors 8, 658–680.
Liu, L., Xu, Z.X., Huang, J.X., 2011. Impact of future climate change on flood in the Xitiaoxi catchment—1. Assessment on VIC model. Resour. Environ. Yangtze Basin 20 (2), 244–250 (in Chinese).
Liu, Z.F., Xu, Z.X., Huang, J.X., Charles, S.P., Fu, G.B., 2010. Impacts of climate change on hydrological processes in the headwater catchment of the Tarim River basin, China. Hydrol. Process. 24, 196–208.
Liuzzo, L., Noto, L.V., Vivoni, E.R., Loggia, G.R., 2010. Basin-scale water resources assessment in Oklahoma under synthetic climate change scenarios using a fully distributed hydrologic model. J. Hydrol. Eng. 15 (2), 107–122.
Lørup, J.K., Refsgaard, J.C., Mazvimavi, D., 1998. Assessing the effect of land use change on catchment runoff by combined use of statistical tests and hydrological modeling: case studies from Zimbabwe. J. Hydrol. 205, 147–163.
Ma, Q.F., 2004. Socio economic driving mechanism research on land use and land cover change in Ya'an city. Master dissertation, Sichuan University, pp. 12–20 (in Chinese).
Mann, H.B., 1945. Non-parametric tests against trend. Econometrica 13, 245–259.
Mao, D.Z., Cherkauer, K.A., 2009. Impacts of land-use change on hydrologic responses in the Great Lakes region. J. Hydrol. 374, 71–82.
Matheussen, B., Kirschbaum, R.L., Goodman, I.A., O'Donnell, G.M., Lettenmaier, D.P., 2000. Effects of land cover change on streamflow in the interior Columbia River basin (USA and Canada). Hydrol. Process. 14, 867–885.
Moiwo, J.P., Lu, W.X., Zhao, Y.S., Yang, Y.H., Yang, Y.M., 2010. Impact of land use on distributed hydrological processes in the semi-arid wetland ecosystem of Western Jilin. Hydrol. Process. 24, 492–503.
Muller, M.R., Middleton, J., 1994. A Markov model of land-use change dynamics in the Niagara Region, Ontario, Canada. Landscape Ecol. 9 (2), 151–157.
Nash, J.E., Sutcliffe, J.V., 1970. Review flow forecasting through conceptual models I: a discussion of principles. J. Hydrol. 10, 282–290.
Niehoff, D., Fritsch, U., Bronstert, A., 2002. Land-use impacts on storm-runoff generation: scenarios of land-use change and simulation of hydrological response in a meso-scale catchment in SW-Germany. J. Hydrol. 267, 80–93.
Pfister, L., Kwadijk, J., Musy, A., Bronstert, A., Hoffmann, L., 2004. Climate change, land use change and runoff prediction in the Rhine–Meuse basins. River Res. Appl. 20, 229–241.
Reynolds, C.A., Jackson, T.J., Rawls, W.J., 1999. Estimating available water content by linking the FAO soil map of the world with global soil profile databases and pedo-transfer functions. In: Proceedings of the AGU 1999 Spring Conference, Boston, MA.
Savary, S., Rousseau, A.N., Quilbé, R., 2009. Assessing the effects of historical land cover changes on runoff and low flows using remote sensing and hydrological modeling. J. Hydrol. Eng. 14 (6), 575–587.
Schilling, K.E., Chan, K.S., Liu, H., Zhang, Y.K., 2010. Quantifying the effect of land use land cover change on increasing discharge in the Upper Mississippi River. J. Hydrol. 387, 343–345.
SRTM 90m Digital Elevation Data, NASA/USGS. <http://srtm.csi.cgiar.org>.
Storck, P., Bowling, L., Wetherbee, P., Lettenmaier, D., 1998. Application of a GIS-based distributed hydrology model for prediction of forest harvest effects on peak stream flow in the Pacific Northwest. Hydrol. Process. 12, 889–904.
Su, F.G., Xie, Z.H., 2003. A model for assessing effects of climate change on runoff of in China. Prog. Natl. Sci. 13 (5), 502–507 (in Chinese).
Turnbull, L., Wainwright, J., Brazier, R.E., 2010. Changes in hydrology and erosion over a transition from grassland to shrubland. Hydrol. Process. 24, 393–414.
VanShaar, J.R., Haddeland, I., Lettenmaier, D.P., 2002. Effects of land-cover changes on the hydrological response of interior Columbia River basin forested catchments. Hydrol. Process. 16, 2499–2520.
Verburg, P.H., Soepboer, W., Veldkamp, A., Limpiada, R., Espaldon, V., Mastura, S.S.A., 2002. Modeling the spatial dynamics of regional land use: the CLUE-s model. Environ. Manage. 30, 391–405.
Xiao, R., Wang, L., Xia, J.G., 2008. Analysis on the changes of arable land areas and social economic driven forces in the mountainous regions of southwestern Sichuan—taking Ya'an city of Sichuan province as an example. Chin. J. Agric. Resour. Regional Plan. 29 (5), 7–12 (in Chinese).
Zhang, L.P., Chen, X.F., Zhang, X.L., Song, X.Y., 2009. A compare application research of VIC model and SWAT model in the mid-small valley flow simulation. Resour. Environ. Yangtze Basin 18 (8), 745–752 (in Chinese).
Zhang, Y.K., Schilling, K.E., 2006. Increasing streamflow and baseflow in Mississippi River since the 1940s: effect of land use change. J. Hydrol. 324, 412–422.
Zhou, S.Q., Liang, X., Chen, J., Gong, P., 2004. An assessment of the VIC-3L hydrological model for the Yangtze River basin based on remote sensing: a case study of the Baohe River basin. Can. J. Remote Sensing 30 (5), 840–853.